IEEE Open Journal of
Power Electronics

Received 1 February 2023; revised 10 March 2023; accepted 16 March 2023. Date of publication 21 March 2023;
date of current version 5 April 2023. The review of this paper was arranged by Associate Editor Qiang Wei.

Digital Object Identifier 10.1109/OJPEL.2023.3260113

Improved Analytical Triple-2D Leakage Inductance Model of Cone Winding Matrix Transformers

RICHARD SCHLESINGER (Student Member, IEEE), AND JÜRGEN BIELA (Senior Member, IEEE)

Laboratory for High Power Electronic Systems (HPE), ETH Zürich, 8092 Zürich, Switzerland

CORRESPONDING AUTHOR: RICHARD SCHLESINGER (e-mail: schlesinger@hpe.ee.ethz.ch)

ABSTRACT The transformer leakage inductance is one of the limiting factors for pulse shape quality in high voltage pulsed power (HVPP) converters that are essential in applications such as cancer treatment, particle accelerators, and free electron lasers. Cone winding matrix (CWM) transformers are commonly used in HVPP converters as they offer low leakage inductance and high insulation distance. This paper proposes an improved Triple-2D (iT2D) leakage inductance model for CWM transformers. The iT2D model identifies three basic cross sections of CWM transformers and calculates their associated leakage inductance contributions. The paper proposes an accurate and compact analytical formula of the leakage inductance contribution resulting from the magnetic energy stored in between the magnetic cores. For cross sections with cone windings, an expression is presented that computes the leakage inductance per unit length of non-parallel windings. The iT2D model is verified with measurements and finite element simulations of three transformer prototypes. The analytical solutions used in the iT2D model ensure applicability to arbitrary geometric aspect ratios and designs. Furthermore, the iT2D model is rapidly executable enabling its time-efficient integration in converter optimisations.

INDEX TERMS Analytical transformer leakage inductance model, cone winding matrix transformer, triple-2D model, transformer parasitics, pulsed power, pulse modulator.

I. INTRODUCTION

High voltage pulsed power (HVPP) converters are key elements in applications such as cancer treatment [1], particle accelerators [2], [3], water treatment and food sterilisation [4], and X-ray free electron lasers for material science [5]. Usually, step-up transformers are used to achieve high voltages at the converter's output. The leakage inductance of these transformers is one of the limiting parasitics that significantly affects pulse shape quality parameters such as rise time and overshoot [6], [7], [8]. In HVPP converters, matrix transformers with cone-shaped high voltage windings as shown in Fig. 1(a) are commonly used [9], [10]. Matrix transformers in pulsed power applications usually describe a transformer with multiple cores and primary windings wound on each core leg whereas two secondary windings enclose all core legs in a row. This concept enables a low product of leakage inductance and parasitic capacitance, resulting in low pulse rise time [2], [6], [9]. Cone windings are used because they offer low leakage inductance and sufficient dielectric insulation distance at the same time [6], [9], [11]. This is because typically both coils are grounded as shown in Fig. 1(b). Therefore, the

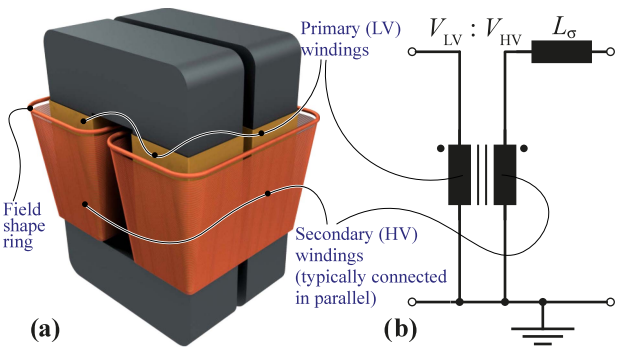

FIGURE 1. (a) Cone winding matrix (CWM) transformer. (b) Typically, both sides are grounded to control the electric field.

top end of the HV-coil reaches high electric potentials with respect to ground in the range of several 100kV resulting in field strengths that are critical for dielectric breakdown. Hence, the top end of the HV-winding is tilted away from the LV-winding to maximise the distance to all neighbouring conducting elements, i.e. core and LV-winding [2]. This cone winding topology has a significantly smaller space between the windings and therefore, a significantly lower leakage inductance compared to conventional parallel windings as the energy of the leakage field is mostly stored in the space between the windings.

In the design process of HVPP converters, the operating and design parameters are often determined with an optimisation before the system is built to save time and costs [7], [12], [13]. In such optimisations, the system parameters are typically recalculated several thousand times (see e.g. [14]). Consequently, the employed models have to be fast as well as accurate to deliver results within a reasonable amount of time. Analytical models are well suited for this purpose as they are typically faster executable than numerical methods such as the finite element method (FEM) [15], [16].

Since the transformer leakage inductance significantly limits the pulse shape quality, it is one of the central design parameters subject to optimisation. Analytically modelling the leakage inductance of cone winding transformers is more complicated than for parallel winding-transformers as the tilted cone winding is not parallel to the other winding and the core edges. This complicates finding a closed form analytical expression of the magnetic field. Existing cone winding transformer leakage inductance models are based on rather strong simplifications and approximations. In [6] and [8], the magnetic field is assumed to be axial (1D-field). This first-order assumption leads to a very compact expression but remains a rather rough approximation of the real magnetic field. Significant errors can result, especially for increasing tilt angles of the cone winding. In [11], mirror images of all separate conductors are used and the leakage inductance is calculated with the method of mean geometric distances (MGD). This method is more accurate but mirroring each conductor individually is computationally quite expensive. Furthermore, this method assumes filamentary currents and neglects the spatial distribution of the current density, which limits accuracy [15]. Also, infinite core permeability is assumed. All analytical models are based on a set of basic transformer cross sections as indicated in Fig. 2(a). All aforementioned models are based on only one cross section [6], [8] or two cross sections [11]. The first considered cross section is the inside-window (IW) cross section shown in Fig. 2(b) and the second cross section is the outside-window (OW) cross section depicted in Fig. 2(c). These two cross sections can also be identified for regular shell-type transformers [15], [16], [17], [18], [19], [20]. Modelling based on IW and OW cross section is often referred to as "Double-2D" concept. However, for accurately and reliably modelling the transformer leakage inductance, it is necessary to take all relevant basic cross sections into account. In the special case of HVPP matrix

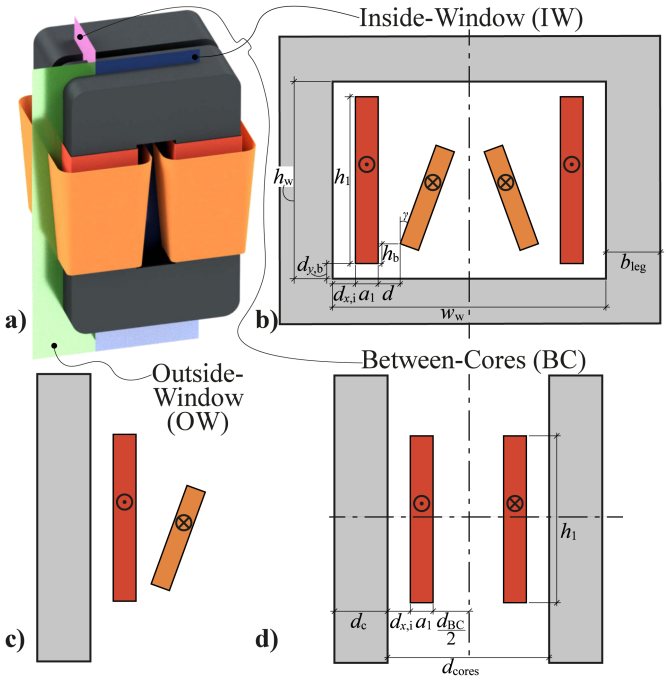

FIGURE 2. (a) Cone Winding Matrix (CWM) transformer & basic cross sections. (b) Inside-Window (IW) cross section. (c) Outside-Window (OW) cross section. (d) Between-Cores (BC) cross section.

transformers, additional magnetic energy is stored between the primary windings of adjacent core legs. Hence, a third cross section can be identified: the Between-Cores (BC) cross section shown in Fig. 2(d).

The authors of this paper recently presented an analytical Triple-2D (T2D) model taking into account all these three basic cross sections and verified the model with one transformer prototype [21]. The T2D model uses a simplified model for the BC cross section assuming axial leakage flux. Assuming purely axial flux, however, leads to errors, especially for transformers with wider and more planar windings because radial flux components become more important. This can become a problem in optimisations as the optimisation algorithm might be misled to designs where the error might be significant. Therefore, a model that considers all cross sections and is also robust towards geometrical variations is required.

This paper presents an improved Triple-2D (iT2D) model that fulfils the aforementioned requirements. The iT2D model is based on the T2D model presented in [21]. The major improvement of the iT2D model is an accurate and fully analytical solution of the leakage inductance contribution of the BC cross section that is developed in this paper. Additionally, the iT2D model uses a more accurate scaling length of the winding corner sections. Furthermore, measurements of two more prototypes with substantially different geometries are added in this paper. Thus, the model is verified with measurements of three transformer prototypes to increase the significance of the verification.

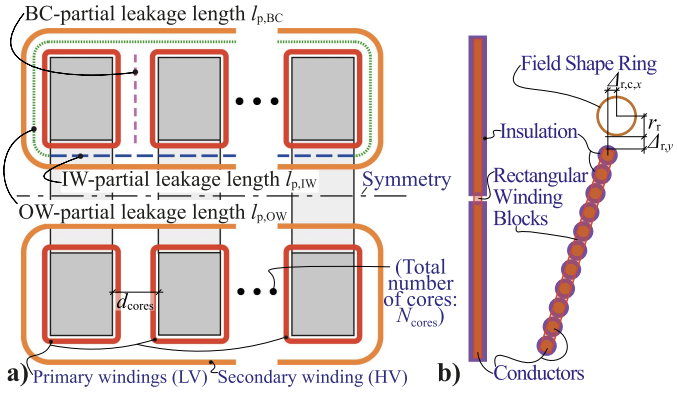

FIGURE 3. **(a) Top view of matrix transformer with arbitrary number of cores and the corresponding cross section scaling lengths. (b) Unified rectangular winding blocks used in the iT2D model are outlined across the outer conductive boundaries of the winding turns.The winding blocks carry a current of *NI*, where *N* is the number of turns of the winding including the field shape ring in case of the secondary winding.**

The paper is organised as follows. Section II explains the basic concept of matrix transformers and its implications for leakage inductance calculations. Next, Section III presents the proposed iT2D model and lists all required equations. Section IV provides a verification of all submodels and the overall model. All model derivations are given in the Appendices.

II. LEAKAGE INDUCTANCE MODELLING OF MATRIX TRANSFORMERS

This section recapitulates the matrix transformer and the Triple-2D leakage inductance modelling concept.

A. MATRIX TRANSFORMER CONCEPT

Matrix transformers comprise several magnetic elements such as cores and windings that are arranged and interconnected in a way such that the total array of components (=matrix) functions as a transformer as a whole [22]. Hence, matrix transformers can denote an infinite set of possible topologies. In high voltage pulsed power converters, matrix transformers are used for step-up operation to achieve secondary voltages up to several hundred kV [5], [6], [11]. These transformers typically consist of multiple cores (often U-cores) with primary windings on each core leg whereas the secondary windings enclose all core legs in a row [2], [6], [7] as shown in Fig. 3(a). With this winding arrangement, two primary windings wound on one core are magnetically coupled with each secondary winding. Hence, the voltage induced in a secondary winding results from the flux caused by two primary windings resulting in a doubled voltage transfer ratio [7]. The secondary windings are usually connected in parallel to decrease the leakage inductance. These matrix transformers feature minimal product of leakage inductance and parasitic capacitance because volume between primary and secondary windings is saved compared to multiple independent interconnected transformers [6]. For generating pulses with lower power, the transformer could also feature only one single secondary winding with primary windings only inside this single secondary winding [2]. To achieve a high voltage on the secondary side, the turn ratio also needs to be quite high, i.e. low number of turns on primary side and high number of turns on the secondary side. To simultaneously achieve a high filling factor and a low number of turns on the primary side, the inner low voltage windings are usually foil windings. Whereas the secondary windings are made of solid round wires with a relatively high number of turns as is shown by the transformers in [2], [10], [23]. Additionally, the winding with the highest electric potential on the HV-side is typically a winding with higher diameter to further decrease the peak electric field, often referred to as field shape ring [2] as depicted in Fig. 1(a). An equivalent circuit model of matrix transformers can be found in [7]. Models to calculate the parasitic transformer capacitance can be found in [24], [25].

B. TRIPLE-2D MODELLING OF MATRIX TRANSFORMERS

The Triple-2D modelling concept is based on three basic cross sections of the matrix transformer: Inside-Window (IW), Outside-Window (OW), and Between-Cores (BC) as shown in Fig. 2. Leakage inductance per unit length L'_σ values are calculated for each cross section and then scaled with the corresponding partial leakage length l_p that are indicated in Fig. 3(a) with dashed lines. Finally, the leakage inductance of matrix transformers can be calculated according to (1).

$$L_\sigma = c_w \left(L'_{\sigma,IW}\, l_{p,IW} + L'_{\sigma,OW}\, l_{p,OW} + L'_{\sigma,BC}\, l_{p,BC} \right) \quad (1)$$

where c_w denotes the electrical interconnection of the secondary windings.

$c_w = 0.5$ for parallel-interconn. secondary windings

$c_w = 2$ for series-interconn. secondary windings

$c_w = 1$ for single-interconn. secondary winding

Note that (1) uses the symmetry regarding the center of the cores highlighted in Fig. 3(a). All leakage inductances are referred to the secondary side in this paper as this is also the convention in the publications of the reference transformers [2], [10], [23] that will be presented in Section IV.

III. IMPROVED TRIPLE-2D (IT2D) LEAKAGE INDUCTANCE MODEL

This section presents the improved Triple-2D (iT2D) model. In particular, the specific submodels are presented which are used for calculating the leakage inductances per unit length (p.u.l.) $L'_{\sigma,BC}$, $L'_{\sigma,OW}$, and $L'_{\sigma,IW}$ and their corresponding partial leakage lengths $l_{p,BC}$, $l_{p,OW}$, and $l_{p,IW}$ required for leakage inductance computation according to (1).

The models are based on the basic relation that a current through an inductance causes a magnetic field that is associated with a certain amount of stored magnetic energy [26]. In particular, leakage inductance L_σ is linked to the magnetic

energy W_{mag} according to

$$L_\sigma = \frac{2W_{\mathrm{mag}}}{I_{\mathrm{ref}}^2}.$$

where I_{ref} is the current through the transformer side that the leakage inductance is referred to. The complete model derivations are given in the Appendices and a detailed derivation of the magnetic energy computed from the magnetic field can be found in [27].

All models are based on unifying the aligned conductors of a winding to a rectangular block whose edges coincide with the outer conductor boundaries neglecting the insulation as shown in Fig. 3(b). This leads to highly reduced computational effort while maintaining high accuracy in leakage inductance calculations [27], [28]. It is to be noted that the diameter of the field shape rings exceeds the diameter of the secondary winding turns by far. Hence, it is inherently difficult to include the field ring geometry in the equivalent rectangular winding blocks. Therefore, the field shape ring is implicitly neglected with the chosen modelling approach. The number of turns of the secondary currents of the unified winding blocks, however, comprise the field shape ring. The decrease in accuracy of assuming a rectangular winding block not containing the field shape ring will be evaluated in Section III-B.

Another consequence of assuming rectangular winding blocks with homogeneous current density is that the model is per definition frequency-independent and skin-& proximity effect are neglected. This is justified for HVPP applications due to the following reasons:

- The transformers are used in pulsed power applications with typically relatively low pulse repetition rates in the range of a few to a few hundred Hz [5], [7], [10], [11]. Hence, a Fourier decomposition of the signal would yield a relatively low fundamental frequency with a certain amount of harmonics. In the circuit simulation of such systems, one can only implement one value for the inductance and since leakage inductance needs to be small to meet the pulse specifications [6], it is reasonable to implement the worst-case inductance value, i.e. the maximal inductance value. At low frequency, inductance is maximal [27], [29], [30], and the iT2D model provides exactly that.
- CWM transformers for HVPP applications always require a significant distance from top of the secondary winding to the inner winding to avoid dielectric breakdowns. Most of the magnetic energy of the leakage field is stored between the windings and this energy is barely affected by frequency since the overall current through the windings does not change with frequency and Ampere's law dictates the field strength between the windings as function of the total current through the windings. Hence, the space between primary and secondary windings limits the drop in inductance of CWM transformers for HVPP applications.

A. BETWEEN-CORES LEAKAGE INDUCTANCE P.U.L.

The leakage inductance per unit length $L'_{\sigma,\mathrm{BC}}$ of the BC cross section is calculated according to (2).

$$L'_{\sigma,\mathrm{BC}} = \frac{8\mu_0 N_2^2 d_{\mathrm{cores}}^4}{a_1^2 h_1^2 \pi^5} \sum_{\substack{n=1 \\ n \text{ is odd}}}^{\infty} \frac{1}{n^4} \left(\frac{\pi h_1}{d_{\mathrm{cores}}} - \frac{1}{n} + \frac{\mathrm{e}^{-n\pi h_1/d_{\mathrm{cores}}}}{n} \right) \left(\sin\left(n \tfrac{\pi}{d_{\mathrm{cores}}} (d_{x,\mathrm{i}} + a_1) \right) - \sin\left(n \tfrac{\pi}{d_{\mathrm{cores}}} d_{x,\mathrm{i}} \right) \right)^2 \quad (2)$$

where μ_0 is the vacuum permeability, N_2 is the number of turns of one secondary winding, and all other variables denote geometrical quantities that are illustrated in Fig. 2. The formula (2) of $L'_{\sigma,\mathrm{BC}}$ is derived analytically in Appendix A using a spatial harmonic Fourier series and solving the Poisson equation by separation of variables. The equation results from a 2D magnetic field expression, hence flux fringing at the top and bottom of the windings is taken into account. Note that the series (2) converges very fast and the summation can be cancelled after summing up a reasonably low number of harmonics, e.g. at $n = 51$ as done in this paper.

B. CONE WINDING LEAKAGE INDUCTANCE P.U.L.

OW and IW cross section of cone winding matrix (CWM) transformers feature non-parallel windings due to the cone-shaped secondary winding, which complicates finding an analytical solution for field and inductance calculations. An accurate and compact model of the leakage inductance per unit length L'_σ of cross sections containing non-parallel windings was proposed in [21] and is also used in this paper. Here, the boundary conditions at the interface between air and the core material are satisfied by using an adequate set of image windings as done in [31] and [15]. The leakage inductance per unit length of IW and OW cross section can then be obtained from (3).

$$L'_\sigma = -\frac{\mu_0}{4\pi} N_2^2 \left[\sum_{i=1}^{2} \frac{\operatorname{sgn} I_i}{a_i h_i} \sum_{k=1}^{N_{\mathrm{wdgs}}} \frac{\operatorname{sgn} I_k}{a_k h_k} \Gamma_{i,k} \right] \quad (3)$$

where i is the index of the original windings, k denotes the index of all windings N_{wdgs}, including mirror image windings, $\Gamma_{i,k}$ is the antiderivate function (27), and a_i & a_k, and h_i and h_k are width and height of winding i and k, respectively. The derivation and all required equations leading to (3) are given in Appendix B.

1) OUTSIDE-WINDOW LEAKAGE INDUCTANCE P.U.L.

In the OW cross section, there is only one mirror resulting in only one set of mirror image windings [15], [32] as shown in Fig. 4(a). The finite relative permeability μ_{r} of the magnetic core is taken into account by multiplying the current of the image windings by the image factor m [32] according to (4)

$$I_{\mathrm{image}} = \underbrace{\frac{\mu_{\mathrm{r}}-1}{\mu_{\mathrm{r}}+1}}_{m} I_{\mathrm{original}}. \quad (4)$$

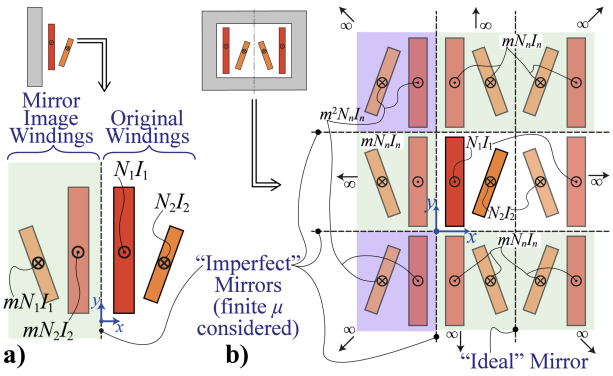

FIGURE 4. (a) Outside-window cross section corresponding to one set of mirror image winding currents with the prefactor $m = \frac{\mu_r - 1}{\mu_r + 1}$. (b) Inside-window cross section is modelled with the eight closest mirror image winding currents. The current prefactors result from taking into account the corresponding boundary conditions.

Referring to (3), this leads to a total of $N_{\text{wdgs}} = 4$ windings in the OW cross section, i.e. two original windings and two mirror image windings as shown in Fig. 4(a).

2) INSIDE-WINDOW LEAKAGE INDUCTANCE P.U.L.

The IW cross section features multiple parallel mirrors, which leads to an infinite number of mirror images [15], [33], [34]. There are infinite mirror images because not only the original windings but also the mirror images are again mirrored at all other mirrors. Previous studies [15], [35] have shown that the eight closest mirror images (one image layer) already lead to satisfactory accuracy, therefore, this paper also uses the eight closest mirror images as shown in Fig. 4(b). The prefactors of the currents of the mirror image windings in Fig. 4(b) result from the following considerations. In the special case of matrix transformers, there are two winding pairs in the IW cross section as shown in Fig. 2(b). Assuming equal currents in the second winding pair leads to a vertical symmetry axis in the center of the IW cross section, which can be exploited in the calculation by only modelling one winding pair, e.g. the left pair. When doing so, it is important that the symmetry line equals a perfect mirroring boundary condition i.e. $\vec{n} \times \vec{H} = \vec{0} \Rightarrow \vec{n} \cdot \vec{A} = 0$. This boundary condition is satisfied by using mirror image winding currents with the same magnitude as the original winding currents, which would also result from a core material with infinite permeability (see "ideal" mirror in Fig. 4(b)). The other three boundaries of the cross section represent interfaces of air and core material with finite permeability. These boundary conditions are modelled by considering the image factor m given in (4) in the mirror image winding currents resulting from the reflections produced by these "imperfect" mirrors. Referring to (3), this leads to a total of $N_{\text{wdgs}} = 18$ windings in the IW cross section.

C. PARTIAL LEAKAGE LENGTH MODELS

As explained in Section II-B, the leakage inductances per unit length L'_σ of each cross section are multiplied by their corresponding partial leakage length to obtain the total leakage inductance contribution of the particular winding section. The partial leakage lengths of BC, OW, & IW cross sections are visualised in Fig. 3(a) and are calculated according to (5)–(7).

$$l_{\text{p,BC}} = (N_{\text{cores}} - 1)\,(b_{\text{leg}} + 2d_{x,\text{i}}) \tag{5}$$

$$l_{\text{p,OW}} = l_{\text{corners}} + 2\,b_{\text{leg}} + N_{\text{cores}}\,d_c + (N_{\text{cores}} - 1)\,d_{\text{cores}} \tag{6}$$

$$l_{\text{p,IW}} = N_{\text{cores}}\,d_c + (N_{\text{cores}} - 1)\,d_{\text{cores}} \tag{7}$$

Where N_{cores} is the number of cores and all other required geometrical quantitites are given in Figs. 2 and 3(a). The corner length l_{corners} comprises four 90°-curved winding sections. In curved winding sections, the magnetic energy is curved and therefore, the scaling length of curved sections has to be radially energy weighted [17], [27]. In the corner length model of the iT2D model, the energy density is assumed to be constant within a rectangle that encloses the windings as provided in Appendix C. The resulting equation is given in (8).

$$l_{\text{corners,iT2D}} = \pi \frac{x_2^2 - d_{\text{x,i}}^2}{x_2 - d_{\text{x,i}}} \tag{8}$$

With $x_2 = d_{\text{x,i}} + a_1 + d + a_2\cos(\gamma) + h_2\sin(\gamma)$, the definition of the parameters can be found in Fig. 2.

IV. VERIFICATION OF IT2D MODEL

This section verifies the iT2D model in two steps. First, the proposed leakage inductance per unit length models and the corner length model presented in the Appendix are verified by comparison with 2D FEM in Sections A–C. Second, the overall iT2D model is verified with measurements in Section D. The two-step verification enables to see the origin of the overall error.

The 2D magnetostatic FEM simulations were performed in Comsol Multiphysics 6.1 with an emphasis on high accuracy, i.e. a manually parametrised very fine mesh – especially in the space between the windings as most of the magnetic energy is stored here. Also, the conductors are modelled with a fine mesh to accuractely capture the magnetic energy density gradients in these regions. Depending on the geometry, the simulations have approximately 300k to 1 million mesh nodes. The minimum element quality in all models is well above the suggested threshold of 0.1 [36]. A sufficient accuracy could have been accomplished even with a much coarser mesh. However, to achieve the most accurate benchmark values for verifying the model, the meshes are parametrised in this elevated level of detail. It is to note that foil windings were meshed with a rectangular mesh such that the angle between mesh lines and expected field gradient is minimal, which minimises interpolation errors along the direction of the field gradient as done in [37]. Mesh plots are spared at this point as the mesh is too fine to be visualised in a reasonable size. The solver settings were kept at default, which triggered the direct MUMPS solver to solve the model.

TABLE 1. Data of the Benchmark Transformers Used for Model Verification. Parameter Definitions See Figs. 2 and 3 and (1)

Misc. parameters							Winding & core dimensions (mm)												Field Ring (mm)		
Trafo	Ref.	N_{cores}	d_{cores}	N_1	N_2	γ	c_{w}	h_{w}	w_{w}	b_{leg}	d_{c}	a_1	a_2	d	h_1	h_2	h_b	$d_{y,\text{b}}$	$d_{x,\text{i}}$	r_{r}	$\Delta_{\text{r,c},x}$	$\Delta_{\text{r},y}$
No.1	[2]	2	50mm	4	124	4.77°	1/2	486	142	233.4	228.6	1	2	12	456	420.5	0	15	3.5	7	0	4.7
No.2	[23]	6	30mm	1	21	17.8°	1/2	302	202	60	140	1	3	40	282	129.2	0	10	4	7	-1.8	3.0
No.3	[10]	2	31mm	1	85	5.35°	1/2	283	95	63	42	0.5	2	5	270	236	-1	6	10	5.5	5.5	0.8

TABLE 2. Results of 2D FEM Simulation, the Proposed iT2D Model, and T2D Model of $L'_{\sigma,\text{BC}}$

	2D FEM	iT2D (2)	T2D [21]
No.1	1708.0 $\frac{\mu\text{H}}{\text{m}}$	-0.04%	3.37%
No.2	39.3 $\frac{\mu\text{H}}{\text{m}}$	-0.01%	3.30%
No.3	338.2 $\frac{\mu\text{H}}{\text{m}}$	-0.18%	2.73%

The verification is based on geometries of three transformer prototypes given in Table 1. These transformers were designed for specific applications, such as the Compact Linear Collider at CERN [2] and the SwissFEL free electron laser at Paul Scherrer Institut [23]. Due to the variation of specifications, the transformer geometries differ accordingly, which enhances the significance of the model verification.

A. VERIFICATION OF BC P.U.L. MODEL

The results of the BC leakage inductance per unit length model (2) derived in Appendix A is compared with 2D FEM in Table 2.The table shows that the error of the proposed model is close to zero, which proves the model derivation to be correct. Additionally, the table shows the error of the simple submodel used for $L'_{\sigma,\text{BC}}$ in the T2D model [21]. Even though the error is rather small for the compared transformer prototypes, the error can be significantly higher in other geometries as the submodel of the T2D model assumes 1D axial flux. The error will increase consistently with smaller and wider windings, i.e. bigger horizontal dimensions and smaller vertical dimensions when referring to Fig. 2(d). In contrary, the proposed model (2) will always deliver very accurate results independent of the geometry as the field solution considers radial as well as axial flux components. The increased robustness towards geometrical variations of the iT2D model is highly beneficial in optimisations as it prevents the optimisation algorithm from being misled to a wrong optimum by a model that does not scale well with geometrical variations. Since matrix transformers can also be of planar type [22], the improved model (2) used in the iT2D model has a clear advantage over the T2D model [21] in this regard.

B. VERIFICATION OF CONE WINDING LEAKAGE INDUCTANCE P.U.L. MODEL

1) OW VERIFICATION

The results of the proposed cone winding leakage inductance per unit length model (3) applied to the OW cross section (1 pair of mirror image windings) is presented in Table 3. The

TABLE 3. Results of the Proposed $L'_{\sigma,\text{OW}}$ Cone Winding Leakage Inductance Model

Model	2D FEM			iT2D (3)
Secondary Conductors	Separate	Unified	Unified	Unified
Field Ring	✓	✓	neglected	neglected
No.1	1349.0 $\frac{\mu\text{H}}{\text{m}}$	-0.31%	0.86%	0.89%
No.2	192.5 $\frac{\mu\text{H}}{\text{m}}$	0.02%	4.06%	4.16%
No.3	657.1 $\frac{\mu\text{H}}{\text{m}}$	-0.28%	1.52%	1.59%

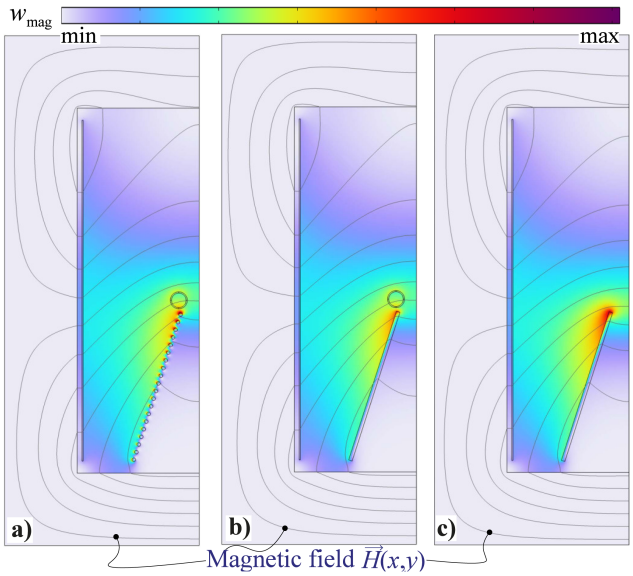

FIGURE 5. 2D-FEM simulation field plot of IW cross section of transformer No.2 [23]. The magnetic energy density w_{mag} is given as coloured surface plot and the magnetic field lines are plotted as black lines. (a) Non-simplified reference geometry with separate conductors and field ring. (b) Unified rectangular winding block and separate field ring. (c) Geometry with the unified rectangular winding blocks only.

benchmark values in the first column of the table relate to the non-simplified geometry of the cross section, i.e. windings modelled as separate conductors and the field ring taken into account as shown in Fig. 5(a).[1] The second column of

[1]Fig. 5 refers to an IW simulation even though the OW simulation results are discussed here. The general conclusions about geometrical simplifications of the windings are universal and are qualitatively independent of the cross section. This is because IW and OW cross sections essentially differ only in their boundary conditions. OW field plots are not shown as the OW simulation domain is too big to be visualised in a reasonable size.

TABLE 4. Results of proposed $L'_{\sigma,\mathrm{IW}}$ cone winding leakage inductance model applied to the IW cross section. The model uses one layer of mirror images corresponding to eight mirror image winding pairs as shown in Fig. 4(b).

Model	2D FEM			iT2D (3)
Secondary Conductors	Separate	Unified	Unified	Unified
Field Ring	✓	✓	neglected	neglected
No.1	1510.0 $\frac{\mu H}{m}$	-0.09%	3.21%	-2.2%
No.2	281.9 $\frac{\mu H}{m}$	0.22%	5.48%	-2.0%
No.3	844.1 $\frac{\mu H}{m}$	0.00%	5.45%	-6.9%

Table 3 results from a simulation that takes the field ring into account but unifies the conductors of the secondary winding to rectangular blocks as shown in Fig. 5(b). The results of this approximation coincide very well with the results of the benchmark geometry, which proves that the unification of windings to rectangular blocks is a very good approximation for leakage inductance calculations, which is also a conclusion in [28]. This conclusion justifies the rectangular winding block assumption of the model presented in Appendix B. The difference in leakage inductance results between the two geometries also manifests in the character of the magnetic energy density distribution shown in Fig. 5. The separate conductors only lead to minor local fluctuations of the energy density around the conductors but the influence on the macroscopic integrated energy per unit length is marginal. Some error is introduced by neglecting the field shape ring, which is shown in the third column of Table 3 that neglects the field shape ring and uses rectangular blocks as secondary windings (cf. Fig. 3(c)). The error of neglecting the field shape ring is in the range of 1% to 4%.

The proposed model (3) provides results that are consistent with the 2D FEM simulation that assumes the same geometry, i.e. unified secondary windings and field shape ring neglected. This confirms the model derivation and implementation to be correct. The error of 1% to 4% is in the acceptable range. Also, neglecting the field ring always leads to an overestimation of the leakage inductance and never an underestimation. This is because neglecting the field ring essentially means assuming a shorter winding, which increases the leakage energy as can be seen in the increased amount of magnetic energy density around the top of the secondary winding block in Fig. 5(c). An overestimation of the leakage inductance is better than an underestimation as it results in a worst-case estimation while the real geometry with field ring will have a lower leakage inductance.

2) IW VERIFICATION

Table 4 shows the results of 2D FEM and the proposed model (3) for the IW cross section. Same as in the OW cross section, some error is introduced by neglecting the field shape ring, which increases the calculated inductance compared to the benchmark value. This assumption and the approximation of using one layer of mirror image winding pairs (cf. Fig. 4(b)) to establish the boundary conditions at the air-core interface lead to an overall error of about 2% to 7% in the IW cross section. The accuracy could be increased by adding more image layers but the error is deemed sufficiently low in this paper and more image layers are avoided to keep the computational effort low.

TABLE 5. Results of scaling length of the corner winding sections l_{corners} calculated with 2D FEM, the proposed model, and the only previously existing model.

	2D FEM (34)	iT2D (8)	T2D [2]
No.1	165.6 mm	8.1%	64.2%
No.2	401.2 mm	-28.5%	29.1%
No.3	172.3 mm	-9.8%	23.0%

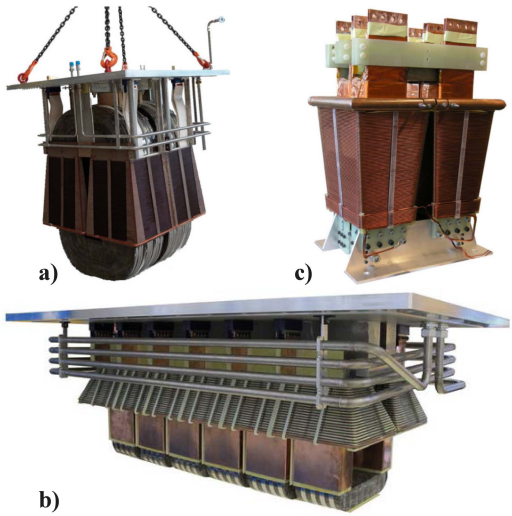

FIGURE 6. Photographs of transformer prototypes (a) No.1 [2]. (b) No.2 [23]. (c) No.3 [10].

C. CORNER LENGTH MODEL

Table 5 shows the error of the proposed corner length model referring to the corner winding sections. The error is non-negligible, however by far lower than the existing corner length model proposed in [2] and also used in the T2D model [21]. The model's benefits are its simplicity consisting of a compact one-line equation and its physically-justified background. There are three reasons for not improving the accuracy of the proposed model. First, the analytic integrations of the magnetic field in (34) would be extraordinarily effortful to derive and to compute. Second, the winding corner lengths are only a fraction of the OW cross section and therefore do not matter significantly in the bigger picture. Third, the bending radii of all turns are equal in existing real CWM transformer prototypes, cf. corner winding sections in Fig. 6. Hence, the axis of rotational symmetry is at a different location for every turn in real transformer prototypes. In contrast, the model and simulation geometry assumes the symmetry axis to be at one constant location leading to an increasing

TABLE 6. Overall error of the proposed iT2D model compared to measurements on existing CWM transformer prototypes. All measurements are related to the secondary (HV) side of the transformer. The column "BC share" represents the share of the leakage inductance contribution of the BC cross section to the total leakage inductance. The measurements of the transformers No.1&2 were taken from the corresponding references [2], [23]. The measurement of transformer No.3 was kindly provided by the author of [10] and was taken at 5 kHz, which yields a good trade-off between high transformer impedance with respect to the output impedance of the impedance analyzer and low impact of skin-& proximity effect.

	Measurement	iT2D	T2D [21]	BC share	Reference
No.1	1325 µH	3.0%	7.6%	15.0%	[2]
No.2	270 µH	5.0%	6.7%	2.4%	[23]
No.3	202 µH	-5.2%	11.1%	7.3%	[10]

bending radius of each winding turn when approaching the field shape ring — which is only a geometrical approximation. Hence, lower model errors do not necessarily translate into a better representation of the existing transformer prototypes in this particular case.

D. VERIFICATION OF OVERALL IT2D MODEL

Table 6 shows leakage inductance measurement results of the three benchmark transformers. The model error is in the range of 3% to 5%. Given that geometrical tolerances and measurement errors can lead to bigger differences, the measurements verifiy the model. Note also that the error of the previous proposed T2D model is slightly higher. Hence, the goal of improving the T2D model [21] has been accomplished with the iT2D model.

It is noteworthy that the share of the leakage inductance contribution of the BC cross section varies between 2% and 15% with the inspected transformer prototypes. That means that the contribution of the BC cross section highly depends on the specific transformer design. Even a hypothetical perfect model would have 15% error in prototype No.1 if it neglected the BC cross section. It is important to point out that the consideration of the leakage inductance contribution of the BC cross section is highly important in optimisations. If not considered, an optimisation algorithm might be misled to a wrong optimum in which the BC cross section contribution is substantial. The iT2D model makes an optimisation immune towards this possible erroneous outcome by providing a highly accurate model of the leakage inductance contribution resulting from the BC cross section, which distincts the iT2D model from the rest of the literature.

V. CONCLUSION

This paper proposes an improved Triple-2D (iT2D) analytical leakage inductance model for cone winding matrix (CWM) transformers. The model uses analytical solutions for each of the three basic transformer cross sections enabling good geometrical scalability. The model is verified with FEM simulations and measurements. The model error compared with the measurements of three benchmark transformer prototypes is between 3% and 5%. This accuracy is satisfactory as geometrical tolerances can lead to errors in similar orders of magnitude.

The execution time on a standard notebook[2] of the iT2D model is in the range of a few milliseconds. This fast execution time combined with its high accuracy make the iT2D model suitable for using it in optimisations of high voltage pulsed power converters. It is especially noteworthy that the iT2D model prevents an optimisation algorithm from being misled towards a wrong optimum by considering all relevant basic transformer cross sections and using accurate models in all these cross sections.

Cone windings enable a significantly lower leakage inductance while keeping the dielectric insulation requirements. Therefore, the iT2D model can be a useful tool for further improving the pulse shape quality of high voltage pulsed power converters.

APPENDIX A
DERIVATION OF BETWEEN-CORES LEAKAGE INDUCTANCE PER UNIT LENGTH MODEL

The Between-Cores cross section equals a field problem, in which two primary windings of equal dimensions are placed symmetrically in a slot enclosed by core material on both sides, cf. Fig. 2(d). Since the core is significantly taller than the windings, assuming the core legs to be infinitely high in this scenario is a very good approximation [15] and will be used in the upcoming solution. Also, the core permeability is assumed to be infinitely high in the BC solution, which is a very good approximation for the leakage field as well. This is because the reluctance path of the leakage field leads through a significant amount of air and the reluctance share of the air is significantly higher than the reluctance share of the core material due to the big difference in magnetic permeability of air ($\mu_{\mathrm{r,air}} = 1$) and core material ($\mu_{\mathrm{r,core}} >> 100$). The assumed configuration is shown in Fig. 7(a). The resulting field in the slot can be represented by a superposition of an infinite number of image winding currents resulting from the adjacent magnetic cores that are modelled by two parallel "ideal" mirrors as indicated in Fig. 7(b). The consequent current density distribution can be represented by a 1D rectangular signal shown in Fig. 7(c). This current density distribution can be approximated with a Fourier series according to (9).

$$\begin{aligned} J_z &= \sum_{n=1}^{\infty} J_n \cos(nqx) \\ &= \sum_{\substack{n=1 \\ n \text{ is odd}}}^{\infty} \frac{4J_{\mathrm{w},1}}{n\pi} \left[\sin(nqx_2) - \sin(nqx_1)\right] \cos(nqx) \end{aligned} \tag{9}$$

where J_n are the Fourier coefficients, $q = \pi/d_{\mathrm{cores}}$, $J_{\mathrm{w},1}$ is the homogeneous current density of the primary winding $J_{\mathrm{w},1} = N_1 I_1/a_1 h_1$ with N_1 being the number of turns of the

[2]Windows 10, Intel i7-8550 U processor, 16 GB RAM, Matlab R2022b

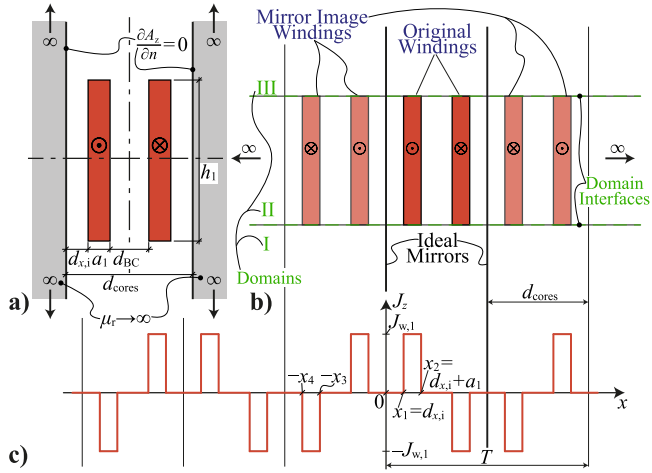

FIGURE 7. Between-Cores model derivation. (a) Mathematical problem. (b) Mathematical equivalent problem with mirrored windings. (c) Consequent current density in domain II as a function of the *x*-coordinate.

primary winding, and I_1 the current through the primary windings. Note that the signal features half-wave symmetry and therefore the even Fourier coefficients become 0 and the corresponding summands vanish. For the domains I–III shown in Fig. 7(b), we can introduce a magnetic vector potential $\vec{A} = A_z(x, y)\vec{e}_z$ as auxiliary quantity to acquire the magnetic flux density $\vec{B} = \vec{\nabla} \times \vec{A}$. From Maxwell's equations, we can derive the Poisson (10a) and the Laplace (10b), respectively for the magnetic potential.

$$\frac{\partial^2 A_z(x,y)}{\partial x^2} + \frac{\partial^2 A_z(x,y)}{\partial y^2} = \begin{cases} -\mu_0 J_z(x), & \text{in II} \quad (10a) \\ 0, & \text{in I \& III.} \quad (10b) \end{cases}$$

From the right hand side of (10a) and using separation of variables, we can assume that the function $A_z(x, y)$ has the shape (11)

$$A_z(x,y) = A_0(y)\cos(nq0) + \sum_{\substack{n=1 \\ n \text{ is odd}}}^{\infty} A_n(y)\cos(nqx). \quad (11)$$

The partial differential equations (PDEs) (10a) & (10b) are solved individually for each odd n-th harmonic of $A_z(x, y)$ and the static part individually, which is valid as the PDEs are linear. The static part $A_0(y)$ can be obtained from the ordinary differential equations

$$\frac{\partial^2 A_0(y)}{\partial y^2} = \begin{cases} -\mu_0 J_0, & \text{in domain II} \quad (12a) \\ 0, & \text{in domains I III.} \quad (12b) \end{cases}$$

Since balanced magnetomotive forces ($N_1 I_1 = -N_2 I_2$) are assumed in leakage inductance calculations [27], $J_0 = 0$. Hence, both (12a) and (12b) can be solved with (13).

$$A_0(y) = \delta_0 + \tilde{\delta}_0 y \quad (13)$$

The coefficient δ_0 can always be set to zero since the magnetic potential is a purely auxiliary quantity and the constant will always drop out after deriving the potential to get a physical field quantity. From Ampere's law, we can conclude that the line integral of the magnetic field strength along the boundary $\oint_{\partial S} \vec{H} \cdot \mathrm{d}\vec{s}$ becomes zero since the sum of the magnetomotive forces is implicitly assumed to be zero in leakage inductance calculations [27]. Therefore, the field cannot contain a constant offset, resulting in $\tilde{\delta}_0 = 0$. Hence, the constant part of the magnetic potential $A_0(y)$ vanishes in all domains.

This leaves the differential equations of the harmonics $A_n(y)$ of the magnetic potential to solve resulting in the ordinary differential equations

$$\frac{\partial^2 A_n(y)}{\partial y^2} = \begin{cases} -\mu_0 J_n, & \text{in domain II} \quad (14a) \\ 0, & \text{in domains I \& III.} \quad (14b) \end{cases}$$

The solution $A_{n,\mathrm{h}}(y)$ to the homogeneous Laplace (14b) can be expressed as [38]

$$A_{n,\mathrm{h}}(y) = \delta_n \mathrm{e}^{nqy} + \tilde{\delta}_n \mathrm{e}^{-nqy}. \quad (15)$$

To solve the inhomogeneous Poisson (14a), a particular solution to the non-homogeneous differential equation has to be added to the homogeneous solution (15). Inserting (15) into (14a), it can be found that the particular solution $A_{n,\mathrm{p}}$ is a constant equal to

$$A_{n,\mathrm{p}} = \frac{\mu_0 J_n}{n^2 q^2}. \quad (16)$$

Hence, the general solutions for $A_n(x, y)$ of all three domains can be found as (17a)–(17c).

$$A_n^{\mathrm{I}}(y) = \alpha_n \mathrm{e}^{nqy} + \tilde{\alpha}_n \mathrm{e}^{-nqy}, \quad \text{in I} \quad (17a)$$

$$A_n^{\mathrm{II}}(y) = \beta_n \mathrm{e}^{nqy} + \tilde{\beta}_n \mathrm{e}^{-nqy} + \frac{\mu_0 J_n}{n^2 q^2}, \quad \text{in II} \quad (17b)$$

$$A_n^{\mathrm{III}}(y) = \gamma_n \mathrm{e}^{nqy} + \tilde{\gamma}_n \mathrm{e}^{-nqy}, \quad \text{in III} \quad (17c)$$

The unknown coefficients can now be determined with boundary and interface counditions. The potential has to be differentiable everywhere, including two hypothetical boundaries infinitely far away at $y \to \infty$ and $y \to -\infty$. Therefore, $\tilde{\alpha}_n = \gamma_n = 0$. The remaining $2(N_D - 1) = 4$ coefficients can be deduced from $2(N_D - 1) = 4$ interface conditions at the domain boundaries, where $N_D = 3$ is the number of domains. In particular, Maxwell's equations dictate two interface conditions per interface

$$B_{\perp,i} = B_{\perp,j} \Rightarrow \partial/\partial x A_{z,i} = \partial/\partial x A_{z,j} \quad (18)$$

$$H_{\parallel,j} - H_{\parallel,i} = K \Rightarrow \mu_j \partial/\partial y A_{z,i} = \mu_i \partial/\partial y A_{z,j}. \quad (19)$$

where i and j denote two adjacent domains, $B_\perp$ is the $\vec{B}$-field component orthogonal at the interface, $H_\parallel$ is the tangential $\vec{H}$-field component, $K = 0$ is the magnitude of the surface current density at the interface and μ is the magnetic permeability. The interface conditions of both interfaces at $y = 0$

and $y = h_1$ result in the coefficients (20)

$$\begin{aligned}\alpha_n &= \tfrac{1}{2}\tfrac{\mu_0 J_n}{n^2 q^2}(1 - \mathrm{e}^{-nqh_1})\\ \beta_n &= -\tfrac{1}{2}\tfrac{\mu_0 J_n}{n^2 q^2}\,\mathrm{e}^{-nqh_1}\\ \tilde{\beta}_n &= -\tfrac{1}{2}\tfrac{\mu_0 J_n}{n^2 q^2}\\ \tilde{\gamma}_n &= \tfrac{1}{2}\tfrac{\mu_0 J_n}{n^2 q^2}(\mathrm{e}^{nqh_1} - 1).\end{aligned} \tag{20}$$

With the magnetic potential at hand, the magnetic field can now be calculated at any given point between the transformer cores. In the present case, the magnetic energy per unit length W'_{mag} is acquired as next step via (21) [27], [33]

$$W'_{\mathrm{mag}} = \frac{1}{2}\iint_{\mathcal{S}} \vec{A}\cdot\vec{J}\,\mathrm{d}A. \tag{21}$$

Since the current density $\vec{J}$ is zero everywhere except in the windings, in which it is also constant, (21) simplifies to (22).

$$\begin{aligned}W'_{\mathrm{mag}} &= \frac{1}{2}\left[J_{\mathrm{w},1}\iint_{\mathrm{wdg}\ 1} A_z^{\mathrm{II}}\,\mathrm{d}A + J_{\mathrm{w},2}\iint_{\mathrm{wdg}\ 2} A_z^{\mathrm{II}}\,\mathrm{d}A\right]\\ &= \frac{J_{\mathrm{w},1}\mu_0}{q^4}\sum_{\substack{n=1\\ n\ \text{is odd}}}^{\infty}\frac{J_n}{n^4}(\sin(nqx_2)-\sin(nqx_1))\left(\mathrm{e}^{-nqh_1}-1+nqh_1\right)\end{aligned} \tag{22}$$

Note that the conditions $J_{\mathrm{w},2} = -J_{\mathrm{w},1}$ and $\sin(nqx_2) - \sin(nqx_1) = -(\sin(nqx_4) - \sin(nqx_3))$ with x_i referring to the winding coordinates given in Fig. 7(c) are used in (22) to notate the solution in the given compact form. Finally, the leakage inductance can be acquired using (23)

$$L'_\sigma = \frac{2W'_{\mathrm{mag}}}{I_{\mathrm{ref}}^2} = \frac{2W'_{\mathrm{mag}}}{I_2^2}. \tag{23}$$

Which after all results in the final equation (2) of the leakage inductance per unit length $L'_{\sigma,\mathrm{BC}}$. It is worth mentioning that the above derivation follows a similar path as the model of Rogowski [33]. However, the underlying geometries differ. In particular, the BC cross section features a high amount of symmetry and no core yokes, leading to several simplifications that lead to a more compact formula. Additionally, the BC cross section features distances $d_{x,\mathrm{i}}$ between the windings and the core legs in contrast to Rogowski's underlying geometry. Furthermore, Rogowski neglected the harmonics of a certain term to shorten the resulting expression. Such a step is consciously avoided in the present derivation as calculating and summing up the harmonics is not a problem with today's electronical computation and neglecting some terms might lead to errors.

APPENDIX B
DERIVATION OF INSIDE-WINDOW & OUTSIDE-WINDOW LEAKAGE INDUCTANCE PER UNIT LENGTH MODEL

The model of $L'_{\sigma,\mathrm{IW}}$ and $L'_{\sigma,\mathrm{OW}}$ is based on calculating the magnetic energy via the z-component of the magnetic potential A_z resulting from an infinitely long rectangular winding k that carries the homogeneous current density $J_{\mathrm{w},k}$ given in

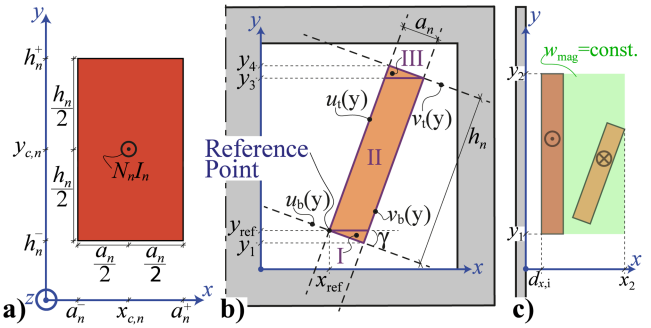

FIGURE 8. (a) Winding parametrisation in parallel coordinate system. (b) Winding parametrisation in non-parallel coordinate system.

(24) according to [39], [40].

$$\begin{aligned}A_{z,k}(x,y) &= -\frac{\mu_0}{4\pi}J_{\mathrm{w},k}F_k\\ &= -\frac{\mu_0}{4\pi}J_{\mathrm{w},k}F(x-x_{\mathrm{c,k}}+w,\,y-y_{\mathrm{c,k}}+s)\Big|_{w=-\frac{a_k}{2}}^{w=\frac{a_k}{2}}\Big|_{s=-\frac{h_k}{2}}^{s=\frac{h_k}{2}}\end{aligned} \tag{24}$$

where $J_{\mathrm{w},k} = \frac{N_k I_k}{a_k h_k}$ is the current density of winding k with N_k being the number of turns, I_k being the winding current, a_k and h_k denote width and height of winding k, respectively, and $x_{\mathrm{c},k}$ and $y_{\mathrm{c},k}$ refer to the center coordinates of the winding k as shown in Fig. 8(a). The function $F(X, Y)$ is given in (25).

$$F(X,Y) = XY\ln(X^2+Y^2) + X^2\arctan\left(\tfrac{Y}{X}\right) + Y^2\arctan\left(\tfrac{X}{Y}\right) \tag{25}$$

The potential function is derived by integrating the source coordinates of a Green's function over the winding dimensions [39], [40]. The Green's function solves the Poisson equation for A_z that describes the potential distribution of the winding embedded in air with the homogeneous permeability μ_0. The magnetic energy per unit length W'_{mag} is calculated using (21). Since the current density is constant over the windings, the integral (21) can be expressed as (26)

$$\begin{aligned}W'_{\mathrm{mag}} &= \frac{1}{2}\left[J_{\mathrm{w},1}\iint_{\mathrm{wdg}\ 1}\sum_{k=1}^{N_{\mathrm{wdgs}}}A_{z,k}\,\mathrm{d}A + J_{\mathrm{w},2}\iint_{\mathrm{wdg}\ 2}\sum_{k=1}^{N_{\mathrm{wdgs}}}A_{z,k}\,\mathrm{d}A\right]\\ &= -\frac{\mu_0}{8\pi}\left[J_{\mathrm{w},1}\iint_{\mathrm{wdg}\ 1}\sum_{k=1}^{N_{\mathrm{wdgs}}}F_k\,\mathrm{d}A + J_{\mathrm{w},2}\iint_{\mathrm{wdg}\ 2}\sum_{k=1}^{N_{\mathrm{wdgs}}}F_k\,\mathrm{d}A\right]\\ &= -\frac{\mu_0}{8\pi}\left[\sum_{i=1}^{2}J_{\mathrm{w,i}}\sum_{k=1}^{N_{\mathrm{wdgs}}}J_{\mathrm{w},k}\Gamma_{i,k}\right]\end{aligned} \tag{26}$$

At this point, it is important to mention that

$$\iint_{\mathrm{wdg}\ i}F_k\,\mathrm{d}A = \iint_{\mathrm{wdg}\ k}F_i\,\mathrm{d}A \Rightarrow \iint_{\mathrm{wdg}\ i}J_{\mathrm{w,i}}A_k = \iint_{\mathrm{wdg}\ k}J_{\mathrm{w},k}A_i,$$

which can be used to avoid having to evaluate some of the integrals.

The integrals in (26) can be analytically evaluated using the antiderivative $\Gamma_{i,k}$, which corresponds to the potential of

winding k integrated over winding i. The antiderivative depends on whether the windings are parallel, or non-parallel.

$$\Gamma_{i,k} = \begin{cases} G_{i,k}, & \text{for parallel windings} \\ \widetilde{G}^{\mathrm{I}}_{i,k} + \widetilde{G}^{\mathrm{II}}_{i,k} + \widetilde{G}^{\mathrm{III}}_{i,k}, & \text{for non-parallel windings.} \end{cases} \tag{27}$$

The antiderivative $G_{i,k}$ in case of parallel windings can be found in [31] as (28).

$$G_{i,k} = G(x - x_{\mathrm{c,k}} + w,\, y - y_{\mathrm{c,k}} + s)\Big|_{w=-\frac{a_k}{2}}^{w=\frac{a_k}{2}}\Big|_{s=-\frac{h_k}{2}}^{s=\frac{h_k}{2}}\Big|_{x=a_i^-}^{x=a_i^+}\Big|_{y=h_i^-}^{y=h_i^+} \tag{28}$$

with the function $G(X, Y)$ given in (29) as proposed in [31].

$$\begin{aligned} G(X,Y) = &-\tfrac{1}{24}(X^4 - 6X^2Y^2 + Y^4)\,\ln(X^2+Y^2) + \tfrac{1}{3}XY \\ &\times \left[X^2 \arctan\left(\tfrac{Y}{X}\right) + Y^2 \arctan\left(\tfrac{X}{Y}\right)\right] - \tfrac{7}{24}X^2Y^2 \end{aligned} \tag{29}$$

In case of non-parallel windings, the integration has to be split in three domains I-III as shown in Fig. 8(b) [21]. Note that typically the secondary windings in CWM transformers are extremely thin and tall. Therefore, domain II is usually by far bigger than domains I & III and therefore, the most determining integral domain. Hence, assuming

$$\Gamma_{i,k} \approx \widetilde{G}^{\mathrm{II}}_{i,k}, \text{ for non-parallel windings}$$

is a very good approximation for thin and tall windings and could be used to speed up the calculation process. Nevertheless, the implementation in this paper does consider the integral contributions of all domains I, II, & III to guarantee geometrical robustness of the model. The antiderivative of one domain $D \in \{\mathrm{I,II,III}\}$ is given in (30)

$$\widetilde{G}^{D}_{i,k} = \widetilde{G}(x, \tilde{x}, y, \tilde{y})\Big|_{\tilde{x}=-x_{\mathrm{c,k}}-\frac{a_k}{2}}^{\tilde{x}=-x_{\mathrm{c,k}}+\frac{a_k}{2}}\Big|_{\tilde{y}=-y_{\mathrm{c,k}}-\frac{h_k}{2}}^{\tilde{y}=-y_{\mathrm{c,k}}+\frac{h_k}{2}}\Big|_{x=u(y)}^{x=v(y)}\Big|_{y=y_{\mathrm{b}}}^{y=y_{\mathrm{t}}} \tag{30}$$

The limits of the outer integral shown in Fig. 8(b) depend on the domain and are given in (31a)–(31c)

$$u(y) = u_{\mathrm{b}}(y) \quad v(y) = v_{\mathrm{b}}(y) \quad y_{\mathrm{b}} = y_1 \quad y_{\mathrm{t}} = y_{\mathrm{ref}} \text{ in I} \tag{31a}$$

$$u(y) = u_{\mathrm{t}}(y) \quad v(y) = v_{\mathrm{b}}(y) \quad y_{\mathrm{b}} = y_{\mathrm{ref}} \quad y_{\mathrm{t}} = y_3 \text{ in II} \tag{31b}$$

$$u(y) = u_{\mathrm{t}}(y) \quad v(y) = v_{\mathrm{t}}(y) \quad y_{\mathrm{b}} = y_3 \quad y_{\mathrm{t}} = y_4 \text{ in III} \tag{31c}$$

The boundary functions $u_{\mathrm{b}}(y)$, $u_{\mathrm{t}}(y)$, $v_{\mathrm{b}}(y)$, and $v_{\mathrm{t}}(y)$ describe the boundaries of the winding and are linear, i.e. they can be expressed as $f(y) = ky + d$, where k is the slope and d is the intercept with the x-axis. The limit function as well as the limits of the y-integration can be taken from (32a)–(32g).

$$u_{\mathrm{b}}(y) = -\cot(\gamma)y + x_{\mathrm{ref}} + \cot(\gamma)y_{\mathrm{ref}} \tag{32a}$$

$$v_{\mathrm{b}}(y) = \tan(\gamma)y + x_{\mathrm{ref}} - \tan(\gamma)y_{\mathrm{ref}} + \tfrac{a_i}{\cos(\gamma)} \tag{32b}$$

$$u_{\mathrm{t}}(y) = \tan(\gamma)y + x_{\mathrm{ref}} - \tan(\gamma)y_{\mathrm{ref}} \tag{32c}$$

$$v_{\mathrm{t}}(y) = -\cot(\gamma)y + x_{\mathrm{ref}} + \cot(\gamma)y_{\mathrm{ref}} + \tfrac{h_i}{\sin(\gamma)} \tag{32d}$$

$$y_1 = y_{\mathrm{ref}} - a_i \sin(\gamma) \tag{32e}$$

$$y_3 = y_{\mathrm{ref}} + h_i \cos(\gamma) - a_i \sin(\gamma) \tag{32f}$$

$$y_4 = y_{\mathrm{ref}} + h_i \cos(\gamma) \tag{32g}$$

And the antiderivative $\widetilde{G}(x, \tilde{x}, y, \tilde{y})$ is given in (33) shown at the bottom of this page. In (33), k equals the slope of the particular boundary function and $\tilde{d} = \tilde{x} + d$ with d being the intercept of the particular boundary function. The antiderivative $\widetilde{G}(x, \tilde{x}, y, \tilde{y})$ is dependent on $\tilde{x}$ and $\tilde{y}$ since the integration contains limits depending on the y-coordinate and therefore the x-integral depends on the y-integral.

An important thing to mention is that the field expressions relate to the coordinate system whose axes are parallel to the winding edges of the current carrying winding k. Hence, the integral limits over the non-parallel winding $u(y)$, $v(y)$, y_{b}, and y_{t} always need to be expressed in the same coordinate system [21].

The magnetic energy per unit length of IW and OW cross section can be calculated using the above listed equations. Finally, the leakage inductance per unit length is calculated using (23), which after all leads to the presented equation (3).

$$\begin{aligned} &\widetilde{G}(x, \tilde{x}, y, \tilde{y}) \\ &= \ln\left(\left(\tilde{d} + k\,y\right)^2 + (y + \tilde{y})^2\right)\left[\left(\tfrac{k^2}{8} - \tfrac{1}{24}\right)y^4 + \left(\tfrac{\tilde{y}\,k^2}{6} + \tfrac{\tilde{d}\,k}{3} - \tfrac{\tilde{y}}{6}\right)y^3 + \left(\tfrac{\tilde{d}^2}{4} + \tfrac{k\,\tilde{d}\,\tilde{y}}{2} - \tfrac{\tilde{y}^2}{4}\right)y^2 + \tfrac{\tilde{y}\left(3\,\tilde{d}^2 - \tilde{y}^2\right)}{6}\,y\right] \\ &\quad - \tfrac{1}{48}y^4\left(7\,k^2 - 1\right) - \tfrac{1}{36}y^3\left(7\,\tilde{y}\,k^2 + 14\,\tilde{d}\,k - 3\,\tilde{y}\right) - \tfrac{1}{24}y^2\left(7\,\tilde{d}^2 + 14\,k\,\tilde{d}\,\tilde{y} - 3\,\tilde{y}^2\right) - \tfrac{1}{12}y\,\tilde{y}\left(7\,\tilde{d}^2 - \tilde{y}^2\right) \\ &\quad + \tfrac{1}{12}y \arctan\left(\tfrac{y+\tilde{y}}{\tilde{d}+k\,y}\right)\left(4\,\tilde{d}^3 + 6\,\tilde{d}^2\,k\,y + 4\,\tilde{d}\,k^2\,y^2 + k^3\,y^3\right) \\ &\quad + \tfrac{1}{12}y \arctan\left(\tfrac{\tilde{d}+k\,y}{y+\tilde{y}}\right)\left(3\,k\,y^3 + 8\,k\,y^2\,\tilde{y} + 4\,\tilde{d}\,y^2 + 6\,k\,y\,\tilde{y}^2 + 12\,\tilde{d}\,y\,\tilde{y} + 12\,\tilde{d}\,\tilde{y}^2\right) \\ &\quad + \tfrac{1}{12\left(k^2+1\right)}\arctan\left(\tfrac{y\,k^2 + \tilde{d}\,k + y + \tilde{y}}{\tilde{d} - k\,\tilde{y}}\right)\left(k\,\tilde{d}^4 + 4\,\tilde{d}^3\,\tilde{y} - 6\,k\,\tilde{d}^2\,\tilde{y}^2 - 4\,\tilde{d}\,\tilde{y}^3 + k\,\tilde{y}^4\right) \\ &\quad - \tfrac{1}{1152\left(k^2+1\right)}\ln\left(\tilde{d}^2 + 2\,\tilde{d}\,k\,y + k^2\,y^2 + y^2 + 2\,y\,\tilde{y} + \tilde{y}^2\right)\left(48\,\tilde{d}^4 - 192\,k\,\tilde{d}^3\,\tilde{y} - 288\,\tilde{d}^2\,\tilde{y}^2 + 192\,k\,\tilde{d}\,\tilde{y}^3 + 48\,\tilde{y}^4\right) \end{aligned} \tag{33}$$

APPENDIX C
DERIVATION OF THE CORNER LENGTH MODEL

As elaborated in [17], [27], the energy weighted mean length required for leakage inductance calculations can be calculated according to (34).

$$l_{\text{corners}} = 2\pi \frac{\iint x\, w_{\text{mag}}\, \mathrm{d}A}{\iint w_{\text{mag}}\, \mathrm{d}A} \tag{34}$$

With w_{mag} as the magnetic energy density and x as the radial coordinate with origin directly at the corner of the core. Since (34) would be quite effortful to compute analytically, the iT2D model uses an approximation of assuming a constant energy density w_{mag} within a rectangle that encloses the windings shown in Fig. 8(c). Inserting the integral boundaries yields

$$l_{\text{corners,iT2D}} = 2\pi \frac{w_{\text{mag}} \int_{y_1}^{y_2} \int_{d_{\text{x,i}}}^{x_2} x\, \mathrm{d}x\mathrm{d}y}{w_{\text{mag}} \int_{y_1}^{y_2} \int_{d_{\text{x,i}}}^{x_2} 1\, \mathrm{d}x\mathrm{d}y}, \tag{35}$$

which results in the provided formula for the corner leakage length in (8).

REFERENCES

[1] S. J. Beebe, "Applications for pulse power using nanosecond pulsed electric fields (nsPEFs) in cell biology and cancer treatment," *J. Nanomedicine Biotherapeutic Discov.*, vol. 3, no. 1, 2013, Art. no. 1000e123.

[2] S. Blume, "Highly efficient pulse modulator system with active droop compensation for linear colliders," Ph.D. dissertation, ETH Zurich, Zurich, Switzerland, 2016.

[3] M. Jaritz, "Solid-state modulator for generating high voltage pulses in the ms-range with high output power," Ph.D. dissertation, ETH Zurich, Zurich, Switzerland, 2018.

[4] H. Akiyama, T. Sakugawa, T. Namihira, K. Takaki, Y. Minamitani, and N. Shimomura, "Industrial applications of pulsed power technology," *IEEE Trans. Dielectrics Elect. Insul.*, vol. 14, no. 5, pp. 1051–1064, Oct. 2007.

[5] D. Gerber and J. Biela, "Design of an ultraprecise 127-MW/3-μs solid-state modulator with split-core transformer," *IEEE Trans. Plasma Sci.*, vol. 44, no. 5, pp. 829–838, May 2016.

[6] D. Bortis, G. Ortiz, J. W. Kolar, and J. Biela, "Design procedure for compact pulse transformers with rectangular pulse shape and fast rise times," *IEEE Trans. Dielectrics Elect. Insul.*, vol. 18, no. 4, pp. 1171–1180, Aug. 2011.

[7] M. Jaritz et al., "A comprehensive design procedure for high voltage pulse power transformers," in *Proc. IEEE Int. Pulsed Power Plasma Sci.*, 2019, pp. 1–4.

[8] D. Habibinia and M. R. Feyzi, "Optimal winding design of a pulse transformer considering parasitic capacitance effect to reach best rise time and overshoot," *IEEE Trans. Dielectrics Elect. Insul.*, vol. 21, no. 3, pp. 1350–1359, Jun. 2014.

[9] H. Lord, "Pulse transformers," *IEEE Trans. Magn.*, vol. 7, no. 1, pp. 17–28, Mar. 1971.

[10] D. Bortis, "20MW halbleiter-leistungsmodulator-system," Ph.D. dissertation, ETH Zürich, Zürich, Switzerland, 2009.

[11] S. Blume and J. Biela, "Optimal transformer design for ultraprecise solid state modulators," *IEEE Trans. Plasma Sci.*, vol. 41, no. 10, pp. 2691–2700, Oct. 2013.

[12] M. Jaritz and J. Biela, "Optimal design of a modular series parallel resonant converter for a solid state 2.88 MW/115-kV long pulse modulator," *IEEE Trans. Plasma Sci.*, vol. 42, no. 10, pp. 3014–3022, Oct. 2014.

[13] S. Blume, M. Jaritz, and J. Biela, "Design and optimization procedure for high-voltage pulse power transformers," *IEEE Trans. Plasma Sci.*, vol. 43, no. 10, pp. 3385–3391, Oct. 2015.

[14] J. Biela and J. W. Kolar, "Pareto-optimal design and performance mapping of telecom rectifier concepts," in *Proc. Power Convers. Intell. Motion Conf.*, 2010, pp. 1–13.

[15] R. Schlesinger and J. Biela, "Comparison of analytical models of transformer leakage inductance: Accuracy vs. computational effort," *IEEE Trans. Power Electron.*, vol. 36, no. 1, pp. 146–156, Jan. 2021.

[16] A. Fouineau, M. A. Raulet, B. Lefebvre, N. Burais, and F. Sixdenier, "Semi-analytical methods for calculation of leakage inductance and frequency-dependent resistance of windings in transformers," *IEEE Trans. Magn.*, vol. 54, no. 10, Oct. 2018, Art. no. 8400510.

[17] R. Schlesinger and J. Biela, "Leakage inductance modelling of transformers: Accurate and fast models to scale the leakage inductance per unit length," in *Proc. Eur. Conf. Power Electron. Appl.*2020, pp. P.1-P.11.

[18] A. F. Hoke and C. R. Sullivan, "An improved two-dimensional numerical modeling method for E-core transformers," in *Proc. IEEE Annu. Appl. Power Electron. Conf. Expo.*, 2002, pp. 151–157.

[19] R. Prieto, J. A. Cobos, O. García, P. Alou, and J. Uceda, "Study of 3-D magnetic components by means of 'double 2-D' methodology," *IEEE Trans. Ind. Electron.*, vol. 50, no. 1, pp. 183–192, Feb. 2003.

[20] M. Mogorovic and D. Dujic, "100 kW, 10 kHz medium-frequency transformer design optimization and experimental verification," *IEEE Trans. Power Electron.*, vol. 34, no. 2, pp. 1696–1708, Feb. 2019.

[21] R. Schlesinger and J. Biela, "Analytical Triple-2D leakage inductance model of cone winding matrix transformers," in *Proc. 23rd Eur. Conf. Power Electron. Appl.*, 2021, pp. P.1-P.10.

[22] E. Herbert, "Design and application of matrix transformers and symmetrical converters," in *Proc. 5th Int. High Freq. Power Convers. Conf.*, 1990, pp. 1–162.

[23] D. A. Gerber, "Ultra-precise short-pulse modulator for a 50MW RF output klystron for free-electron lasers," Ph.D. dissertation, ETH Zurich, Zurich, Switzerland, 2015.

[24] J. Biela and J. W. Kolar, "Using transformer parasitics for resonant converters - A review of the calculation of the stray capacitance of transformers," *IEEE Trans. Ind. Appl.*, vol. 44, no. 1, pp. 223–233, Jan./Feb. 2008.

[25] H. Singer, H. Steinbigler, and P. Weiss, "A charge simulation method for the calculation of high voltage fields," *IEEE Trans. Power App. Syst.*, vol. PAS-93, no. 5, pp. 1660–1668, Sep. 1974.

[26] J. D. Jackson, *Classical Electrodynamics*, 3rd ed., Hoboken, NJ, USA: Wiley, 1999.

[27] R. Schlesinger, T. Ewald, and J. Biela, "Analytical hybrid Quasi-3D transformer leakage inductance model," *IEEE Trans. Power Electron.*, vol. 38, no. 4, pp. 5092–5106, Apr. 2023.

[28] A. Sharma and J. W. Kimball, "Evaluation of transformer leakage inductance using magnetic image method," *IEEE Trans. Magn.*, vol. 57, no. 11, Nov. 2021, Art. no. 8401912.

[29] A. Van den Bossche and V. C. Valchev, *Inductors and Transformers for Power Electronics*. Boca Raton, FL, USA: CRC Press Taylor & Francis Group, 2005.

[30] P. Dowell, "Effects of eddy currents in transformer windings," *Proc. Inst. Elect. Eng.*, vol. 113, no. 8, 1966, Art. no. 1387.

[31] X. Margueron, A. Besri, P. O. Jeannin, J. P. Keradec, and G. Parent, "Complete analytical calculation of static leakage parameters: A step toward HF transformer optimization," *IEEE Trans. Ind. Appl.*, vol. 46, no. 3, pp. 1055–1063, May/Jun. 2010.

[32] P. Hammond, "Electric and magnetic images," *Proc. IEE - Part C: Monographs*, vol. 107, no. 12, pp. 306–313 1960.

[33] W. Rogowski, "Ueber das streufeld und den streuinduktionskoeffizienten eines transformators mit scheibenwicklung und geteilten endspulen," Ph.D. dissertation, Technische Hochschule zu Danzig, Danzig, Germany, 1908.

[34] E. Roth, "Étude analytique du champ de fuites des transformateurs et des efforts mécaniques exercés sur les enroulements," *Revue générale de l'électricité*, vol. 23, pp. 773–787, 1928.

[35] M. Lambert, F. Sirois, M. Martinez-Duro, and J. Mahseredjian, "Analytical calculation of leakage inductance for low-frequency transformer modeling," *IEEE Trans. Power Del.*, vol. 28, no. 1, pp. 507–515, Jan. 2013.

[36] H. Gothäll, "How to inspect your mesh in COMSOL multiphysics," 2022. [Online]. Available: https://www.comsol.com/blogs/how-to-inspect-your-mesh-in-comsol-multiphysics/

[37] T. B. Gradinger, U. Drofenik, and F. Grecki, "Enabling foil windings of medium-frequency transformers for high currents keywords," in *Proc. IEEE 22nd Eur. Conf. Power Electron. Appl.*, 2020, pp. 1–10.

[38] K. Binns and P. Lawrenson, *Analysis and Computation of Electric and Magnetic Field Problems*, 2nd ed., Oxford, U.K.: Pergamon Press, 1973.

[39] M. Strütt, "Das magnetische feld eines rechteckigen, von gleichstrom durchflossenen leiters," *Archiv für Elektrotechnik*, vol. 17, no. 5, pp. 533–535, 1926.
[40] X. Margueron, J. P. Keradec, and D. Magot, "Analytical calculation of static leakage inductances of HF transformers using PEEC formulas," *IEEE Trans. Ind. Appl.*, vol. 43, no. 4, pp. 884–892, Jul./Aug. 2007.

RICHARD SCHLESINGER (Student Member, IEEE) received the Dipl.-Ing. degree (M.Sc. equivalent) (with distinction) in energy and environmental technology from TU Wien, Vienna, Austria, in 2018. Since 2018, he has been working toward the Ph.D. degree with the Laboratory for High Power Electronic Systems, ETH Zurich, Zürich, Switzerland. In his master's thesis he modelled and evaluated three-terminal impedance measurement setups for solid oxide fuel cell electrodes. His research interests include modeling and design of magnetic components with special focus on analytical modelling of the transformer leakage inductance. In 2021, he was the recipient of the EPCIA Student Paper Award for his paper entitled Analytical Triple-2D Leakage Inductance Model of Cone Winding Matrix Transformers.

JÜRGEN BIELA (Senior Member, IEEE) received the Diploma (with Hons.) from Friedrich-Alexander Universität Erlangen-Nürnberg, Erlangen, Germany, in 1999, and the Ph.D. degree from the Swiss Federal Institute of Technology, ETH Zürich, Zürich, Switzerland, in 2006. In 2000, he joined the Research Department, Siemens A&D, Erlangen, and in 2002, the Power Electronic Systems Laboratory, ETH Zürich, as a Ph.D. student focusing on electromagnetically integrated resonant converters. From 2006 to 2010, he was a Postdoctoral Fellow with the Power Electronic Systems Laboratory. Since 2010, he has been an Associate Professor and since 2020, a Full Professor of high-power electronic systems with ETH Zurich.